Central Transition Nuclear Magnetic Resonance in the Presence of Large Quadrupole Couplings: Cobalt-59 Nuclear Magnetic Resonance of Cobaltophthalocyanines†

Ales Medek, Veronica Frydman, and Lucio Frydman*

Department of Chemistry, M/C 111, University of Illinois at Chicago, 845 West Taylor Street, Chicago, Illinois 60607-7061

Received: February 3, 1999

The acquisition of distortion-free solid-state nuclear magnetic resonance (NMR) powder line shapes from half-integer spin systems possessing large quadrupole couplings is exemplified on cobaltophthalocyanine complexes. The acquisition of ideal-like static line shapes even for megahertz-wide central transition patterns is discussed, with the aid of spin−echo sequences incorporating short and very weak radio frequency (rf) pulses. Under these conditions most of the crystallites within the bandwidth of interest are excited with essentially orientation-independent pulse angles, while the acquisition of several experiments with varying carrier frequency offsets alleviates the limited bandwidth of the excitation given by the rf pulse lengths. After this approach was tuned with the aid of quantum mechanical calculations and model compounds, it was applied to the study of diamagnetic metal centers in hexacoordinated Co(III)phthalocyanines. Solid-state ^{59}Co NMR spectra were acquired as a function of the external magnetic field on complexes with general structure $[(L)_2CoPc]Br$, where Pc denotes the phthalocyanine macrocycle and the axial ligands L were pyridine, methylimidazole, methylpiperidine, and ammonia. Iterative numerical fittings of these data revealed anisotropic coupling parameters that were larger than those observed in cobaltoporphyrin analogues but, which like the latter, deviated from trends traditionally observed for nonaromatic octahedral cobalt complexes. These systematic differences observed for the various ^{59}Co coupling parameters are discussed.

1. Introduction

A majority of NMR-active nuclides possess spin numbers larger than 1/2 and are therefore affected by the quadrupolar interaction.[1,2] This electric coupling depends on the local symmetry surrounding the nuclear site[1−3] and in many instances can be comparable to the Zeeman interaction between the nuclear magnetic moments and the external magnetic field. Under such conditions the NMR resonances of the sites tend to be substantially broadened: in solution because of efficient quadrupolar relaxation and in the solid state because of the anisotropic character of the quadrupolar coupling.[4] In the latter phase, however, the broadenings are inhomogeneous and thereby in principle reversible, and since for half-integer nuclides they do not affect the central $-1/2 \leftrightarrow +1/2$ transition to first order, the prospects of observing these signals are good. Unfortunately, in many cases even these central transitions are substantially broadened due to second-order quadrupole effects.[1−5] A relevant question that may then arise is how can meaningful NMR spectra be acquired in the presence of large quadrupolar coupling constants? The present work addresses this issue and exemplifies it with a ^{59}Co NMR study of diamagnetic cobaltophthalocyanine complexes.

A common approach employed in solid-state spin-1/2 spectroscopy to deal with NMR spectral broadenings is to mechanically average the anisotropies by means of magic-angle spinning (MAS).[6,7] Although conventional fixed-angle rotation techniques such as MAS are unable by themselves to remove second-order anisotropies,[8] they can be extended into more complex multiple-axes spinning techniques or combined with multiple-quantum spectroscopy to completely eliminate broadenings of quadrupolar origin.[9−12] It has been our experience, however, that when very large quadrupole couplings are involved and central transition second-order effects exceed by far the rate of sample rotation, neither MAS nor any of its usually less-sensitive high-resolution variants are really helpful for enabling the observation of central transition quadrupole resonances. This is in contrast to what happens with spin-1/2 nuclei acted by shielding anisotropy, where patterns break into sharp sidebands even at slow spinning rates,[13,14] and it is probably a consequence of MAS's inability to prevent the rapid quadrupole-induced dephasing. Eventually it is likely that these problems will be overcome by increasingly strong magnetic field strengths (which scale second-order effects) and by faster spinning rotors, but in the meantime they circumscribe quantitative observations under the effects of large quadrupole couplings to static low-resolution conditions. This is the kind of situation that we faced during the course of ^{59}Co NMR studies on organometallic Co(III) complexes.[15,16] This is an abundant and relatively sensitive isotope possessing a spin number $S = 7/2$,[17] but it can be subject to relatively large quadrupole couplings with e^2qQ/h constants in the 10−100 MHz range. To deal with the ensuing broadenings a protocol was developed and applied to static ^{59}Co NMR studies of cobaltoporphyrins, cobaloximes, and cobalamines; we present here the technical details underlying this approach and illustrate it with a series of applications to cobaltophthalocyanines.

Phthalocyanine complexes possess a number of important applications and have consequently been the focus of extensive basic and applied chemical investigations.[18−20] Their intense green-blue color combined with outstanding chemical, thermal, and radiation stabilities have made these and other metallophthalocyanines essential pigments for a wide variety of dyes,

† Presented in part at the 39th Experimental NMR Conference, Asilomar, CA, 1998; Poster 159.

10.1021/jp990410d CCC: $18.00
Published on Web 05/25/1999

CHART 1

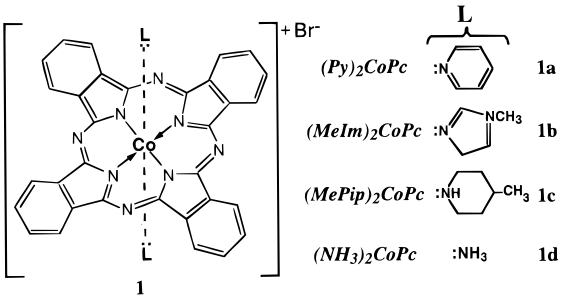

1

lacquers, and inks.[21] The combination of extreme stability with nonlinear optical behavior and extensive electron delocalization also endows these compounds with valuable promise as optoelectronic constituents in switches, modulators, and data storage,[22,23] while their organic nature has also prompted their incorporation into conventional and liquid-crystalline polymer materials.[24,25] From the NMR spectroscopy standpoint the study of these compounds has been problematic due to their general insolubility; solid-state analyses are naturally free from this complication[26,27] and are made further relevant by the solid-phase character of most metallophthalocyanine applications. Among the various spectroscopic probes available to study cobaltophthalocyanines, ^{59}Co is a most promising one, thanks to the close relations that connect the quadrupolar and shielding couplings of this metal with its surrounding electronic environment.[28−30] A series of such complexes was thus synthesized for these spectroscopic studies, incorporating axial substituents that could stabilize the diamagnetic Co(III) $3d^6$ electronic state and thereby allow their study by metal NMR. Upon choosing the axial substitution patterns required by these complexes, consideration was given to the structurally similar cobaltoporphyrins whose ^{59}Co NMR data we have recently reported;[16] as a result of this ^{59}Co NMR coupling tensors in phthalocyanines could be analyzed independently as well as in comparison with relevant analogues. The differences and similarities observed are discussed in terms of the structural and electronic mechanisms that dictate the ^{59}Co parameters in these compounds.

2. Materials and Methods

Co(III) Complexes: Preparation. All chemicals employed in the present study were purchased from Aldrich. These include $K_3[Co(CN)_6]$ and $Co(acac)_3$, model compounds which were analyzed by NMR without further processing, as well as the anhydrous solvents chloroform, pyridine, benzene, and methanol and the precursors bromine, Co(II)phthalocyanine, ammonia (2.0 M solution in methanol), 4-methylpiperidine, and *N*-methylimidazole used in the synthesis of the cobaltophthalocyanines. The structures of the various $[(L)_2CoPc]^+Br^-$ complexes that were prepared are shown in Chart 1. Compounds **1b**−**1d** were synthesized according to the method developed by Vollmann et al.;[31,32] in each case Co(II)phthalocyanine was oxidized with bromine affording the dibromo compound $[CoPc]Br_2$, which was subsequently treated with the corresponding ligand L. Compound **1a** was obtained using a reverse sequence in which Co(II)phthalocyanine was treated with pyridine to form the complex $(Py)_2CoPc$, which was then oxidized with bromine. The final products were identified by 200 or 400 MHz ^{1}H NMR, by 75.8 MHz ^{13}C high-resolution solid-state NMR, and by elemental analysis (Midwest Microlab, Indianapolis, IN).

NMR Measurements. ^{59}Co NMR spectra were acquired at two magnetic field strengths, 4.7 and 11.8 T (48 and 120 MHz Larmor frequencies), to remove ambiguities that may otherwise affect the determination of shielding and quadrupole tensors in central transition determinations. These spectrometers were equipped with laboratory-built consoles and static sample probeheads capable of achieving radio frequency (rf) irradiation fields in excess of 100 kHz. The instrumental dead times of both spectrometers were shorter than 20 μs. The NMR signal arising from a 1 M aqueous $K_3[Co(CN)_6]$ solution was used as external standard for referencing all the ^{59}Co NMR measurements. To overcome the effects of the spectrometer dead time, signals were acquired using the two-pulse sequence schematized in Figure 1, with the whole echo being acquired for the sake of signal-to-noise improvement; 50 μs echo delay times and 100 ms recycle times were generally used in the spectral acquisitions; further pulse sequence details are given and justified in the following paragraphs. Typically four to six time-domain signals with 100 000 scans each and irradiation carrier offsets varied by 100 kHz were chosen to evenly cover the whole powder pattern line width. The numerical simulations of the experimental data were performed on Sun Ultrasparc and Macintosh PowerPC computers using specially written C language programs.

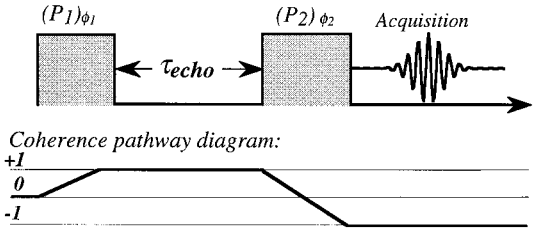

Figure 1. Two-pulse spin−echo sequence employed in the acquisition of static ^{59}Co NMR data. The indicated coherence transfer pathway was selected by means of a standard 8-scan cycle where the phase ϕ_1 of the first pulse was incremented by 90° and the phase ϕ_2 was cycled as $\phi_1 \pm 90°$.

NMR Theory and Simulations. Prior to describing the details of the pulse sequences that were used and the ^{59}Co NMR results observed, it is convenient to summarize the main spectroscopic considerations that were taken into account in these experiments. The internal Hamiltonian considered for describing the behavior of the spins in the absence of rf irradiation was[1,2]

$$H_{\text{int}} = H_{\text{offset}} + H_{\text{Q}}^{(1)} + H_{\text{Q}}^{(2)} + H_{\text{CSA}} \tag{1}$$

where the first term represents possible rotating-frame frequency offsets, $H_{\text{Q}}^{(1)}$ and $H_{\text{Q}}^{(2)}$ are the first- and second-order quadrupole effects, and H_{CSA} is the chemical shift anisotropy. Since internal couplings are tensorial properties, the most convenient way to describe them is in terms of irreducible spherical tensor operators[2,33]

$$H_{\text{Q}}^{(1)} = C_{\text{Q}} T_{20}^{\text{Q}} R_{20}^{\text{Q}} \tag{2a}$$

$$H_{\text{Q}}^{(2)} = -\frac{C_{\text{Q}}^2}{\omega_{\text{L}}} \sum_{m=1}^{2} \frac{[T_{2m}^{\text{Q}}, T_{2-m}^{\text{Q}}]}{m} R_{2m}^{\text{Q}} R_{2-m}^{\text{Q}} \tag{2b}$$

$$H_{\text{CSA}} = C_{\text{CSA}} \sum_{m=-2}^{2} (-1)^m T_{2m}^{\text{CSA}} R_{2-m}^{\text{CSA}} \tag{2c}$$

where T_{lm}^{i} and R_{lm}^{i} represent the spin and spatial parts and C_i is the coupling constant characterizing the various Hamiltonians. To calculate actual transition frequencies, the principal axes

systems (PASs) of these shielding and quadrupolar interactions need to be related by a fixed set of Euler angles (α,β,γ), while an arbitrary powder orientation (θ,φ) will align these molecular PASs with respect to the laboratory frame given by the external magnetic field. These transformations can be conveniently defined as[34]

$$\mathrm{PAS_{CSA}} \xrightarrow{(\alpha,\beta,\gamma)} \mathrm{PAS_Q} \xrightarrow{(\theta,\varphi)} \text{lab frame} \qquad (3)$$

which are accounted for in the actual calculation by Wigner rotation matrixes $\{D_{m'm}^{(l)}\}$.[33] By computing suitably weighted averages for the eigenvalues arising from this internal Hamiltonian, such model was employed to calculate the ideal NMR frequency powder line shapes arising from the central $+1/2 \leftrightarrow -1/2$ ^{59}Co central transitions. These expressions were also used in the fine-tuning of a pulse sequence capable of affording such ideal line shapes, by employing them in the explicit time propagation of the nuclear spin density matrix. In this case the effects of the two rf pulses in a spin−echo sequence (Figure 1) were computed by superimposing on the internal couplings an rf Hamiltonian

$$H_{\mathrm{rf}}(t) = \begin{cases} \nu_{\mathrm{rf}} S_{\phi_i} & \text{during pulses } P_1, P_2 \\ 0 & \text{during free evolution} \end{cases} \qquad (4)$$

where the $\{\phi_i\}$ corresponds to the suitably cycled phases of each pulse. From the total Hamiltonian $H_{\mathrm{int}} + H_{\mathrm{rf}}$ the evolution of the spin ensemble was calculated as

$$\rho(t) = U^{-1}(t) S_z U(t) \qquad (5)$$

where the time propagator

$$U(t) = U(P_1)\cdot U(\tau_{\mathrm{echo}})\cdot U(P_2)\cdot U(t_{\mathrm{acq}}) \qquad (6)$$

accounts for the evolution during the first pulse, the echo period, the second pulse, and the acquisition time, respectively. The final signal *S(t)* detected was then assumed to arise solely from the central $-1/2 \leftrightarrow +1/2$ transition and computed from the corresponding fictitious spin-1/2 operator

$$S(t) = Tr[\rho(t)\cdot S_+^{-1/2\leftrightarrow+1/2}] \qquad (7)$$

Because a full echo (i.e., τ_{echo} > signal powder lifetime) was acquired in the actual experiments, time-domain data could be processed into purely absorptive spectra simply by carrying out a magnitude calculation of the suitably weighted Fourier transforms. All subsequent manipulations (such as spectral coaddition) were then carried out on these frequency domain data.

Pulse Sequence Optimization. When attempting the acquisition of undistorted solid-state NMR spectra spanning a considerable bandwidth, the ideal scheme would involve a spin−echo sequence based on infinitely strong δ pulses. Since this is obviously unfeasible, the question arises on which is the best practical solution. Extensive research on the question of the application of spin−echoes to half-integer quadrupoles has been carried out.[35−40] As noted in these and in other previous works, the main complications of this manipulation are the strong nutation effects that depend both on the strength ν_{rf} of the rf field and on the orientation-dependent frequency $\nu_{\mathrm{Q}}(\theta,\varphi)$ defining the first-order quadrupole interaction.[41,42] Only in the extreme cases $\nu_{\mathrm{rf}} \gg \nu_{\mathrm{Q}}$ or $\nu_{\mathrm{rf}} \ll \nu_{\mathrm{Q}}$ for all (θ,φ) angles does the excitation of the powder become orientation-independent, and since for systems with moderate-to-large quadrupole couplings

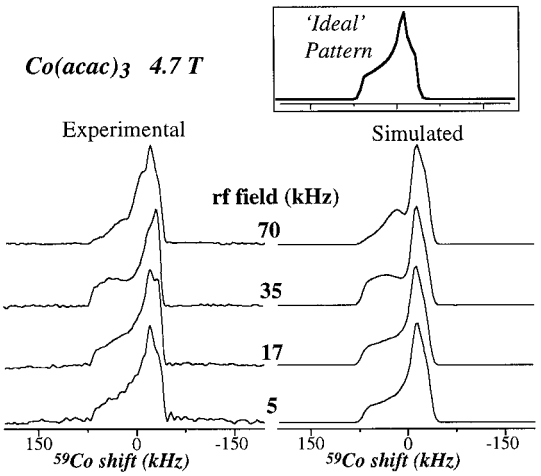

Figure 2. Radio frequency field dependence observed for the static ^{59}Co NMR spectrum of Co(acac)$_3$. Experimental NMR data were collected at 47.7 MHz using the sequence in Figure 1 (3 μs pulses), on-resonance irradiation, $\tau_{\mathrm{echo}} = 220$ μs, 200 kHz spectral width, 300 ms recycling delay, and 2000 scans. rf field strengths were calibrated using a $K_3[Co(CN)_6]$ solution. The simulations on the right arise from a time-domain propagation of the $S = 7/2$ density matrix throughout the various steps of a sequence involving the indicated experimental conditions and the ^{59}Co coupling parameters reported by Eichele et al. ($e^2qQ/h = 5.53$ MHz, $\eta_{\mathrm{q}} = 0.22$, $\delta_{\mathrm{CSA}} = 698$ ppm, $\eta_{\mathrm{CSA}} = 0.36$) on the basis of a single-crystal rotation analysis.[43] The inset illustrates the ideal central transition powder line shape expected from these parameters after convolution with an 800 Hz artificial line broadening.

such as the ones under consideration the strong irradiation condition is nearly impossible to fulfill, the use of very weak rf fields becomes the safest choice to obtain undistorted powder spectra. In fact the acquisition of ideal-like powder patterns may require unusually weak rf fields, as illustrated in Figure 2 for the model compound Co(III)acetylacetonate. Even though the ^{59}Co quadrupolar coupling constant in this complex is relatively small, it was not possible to meet the high-field conditions with the available rf field strengths, and only when rf fields were weaker than ca. 5 kHz did spins in the majority of crystallites precess at the same rate and thereby originate undistorted powder line shapes.

Faced with the need to use such relatively weak rf fields, an important consideration becomes the choice of optimal pulse lengths. Sensitivity would benefit if weak rf fields were used in combination with relatively long pulses, but this in turn would lead to severely narrow excitation bandwidths which could become themselves a source of line shape distortion. Short pulses capable of exciting homogeneously very wide central transitions would not be a practical choice either as they would entail negligible excitation angles. As a compromise between these two extremes, we found it convenient to employ ca. 3 μs long pulses corresponding to nutation angles for which sufficient signal can be rapidly collected, while keeping the spin manipulations essentially orientation-independent. To deal with the limited excitation bandwidth characterizing even these short pulses, a frequency-swept irradiation procedure similar to the one described by Massiot et al. was adopted:[38] since 3 μs pulses excite with a flat profile a region of approximately $\pm$100 kHz around the carrier frequency offset, collecting a series of subspectra separated by 100−150 kHz offsets enables the faithful characterization of central transition line shapes without redundant acquisitions. The suitability of this procedure is illustrated in the left-hand column of Figure 3, which presents a series of variable offset ^{59}Co NMR acquisitions on one of the cobaltophthalocyanine complexes prepared for this study. In

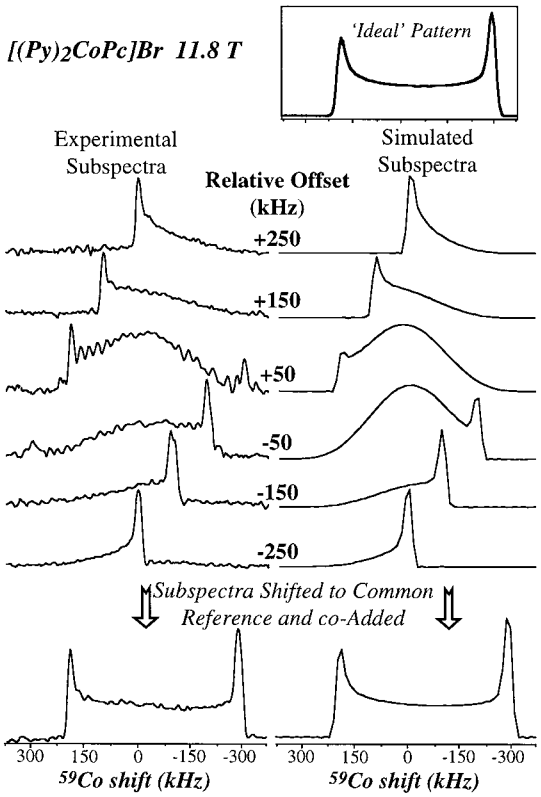

Figure 3. 120 MHz ^{59}Co NMR line shapes resulting from [(Py)$_2$CoPc]-Br as a result of variable offset spin−echo data acquisitions. The experimental subspectra (left) were obtained as indicated in Figure 2 but using a 5 kHz rf field, $\tau_{echo} = 50\ \mu$s, 100 ms recycle delay, spectral width of ±500 kHz, and 100 000 scans. The offsets indicate the position of the rf carrier with respect to the ^{59}Co NMR peak of the complex in a saturated pyridine solution, which appears at 9470 ppm downfield from $K_3[Co(CN)_6]$ with a half-line-width of 13.8 kHz. An ideal fit of the total experimental spectrum (inset) yields coupling parameters which were in turn employed to calculate the intermediate subspectra shown on the right via an explicit time propagation of the spin density matrix.

these experiments the echo delay between the two rf pulses was set long enough to ensure the acquisition of the complete spin−echo, yet not longer than essential in order to achieve maximum sensitivity. After all the subspectra were processed and shifted to a common reference frequency, their coaddition yielded an experimental trace which could be fitted to extract the site's quadrupolar and shielding parameters using the idealized H_{int} coupling Hamiltonian (Figure 3, top). As further proof on the nearly ideal line shapes that this approach is expected to yield, the right-hand column of Figure 3 shows the predictions arising from a rigorous quantum-mechanical time propagation of the spin density matrix for the quadrupolar and shielding parameters extracted from the experimental powder pattern and for the various rf amplitudes, timing, phases, and offsets employed. As can be appreciated the trace that results from the coaddition of these subspectra closely resembles the experimental pattern and is almost indistinguishable from the ideal powder simulation.

3. Results and Discussion

The approach described in the preceding section was employed to extend our previous solid-state ^{59}Co NMR observations on cobalamines, cobaloximes, and cobaltoporphyrins to the study of cobaltophthalocyanines. As in those previous analyses measurements were repeated as a function of magnetic field strength in order to better discriminate between shielding

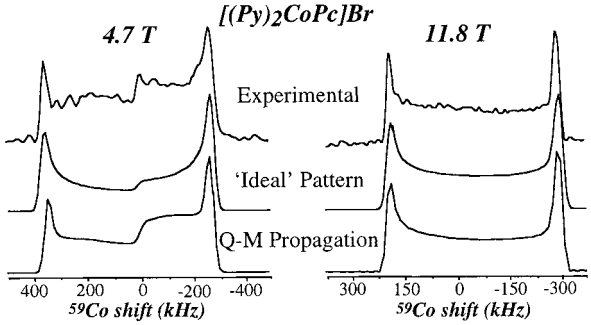

Figure 4. Field dependence observed for the solid-state ^{59}Co NMR spectrum of [(Py)$_2$CoPc]Br. Experimental data were collected as described in Figure 3, using similar acquisition conditions at both magnetic field strengths. The "ideal" line shapes correspond to best fits of the experiments using the coupling parameters listed in Table 1 and the Hamiltonians given in eqs 1 and 2; the quantum mechanical simulations (bottom) employed these parameters to reconstruct the expected line shape from explicit time propagations of the density matrix.

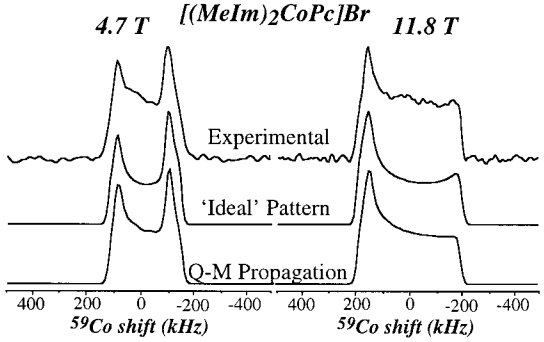

Figure 5. Field dependence observed for the solid-state ^{59}Co NMR spectrum of [(MeIm)$_2$CoPc]Br. Data are as described in Figure 4.

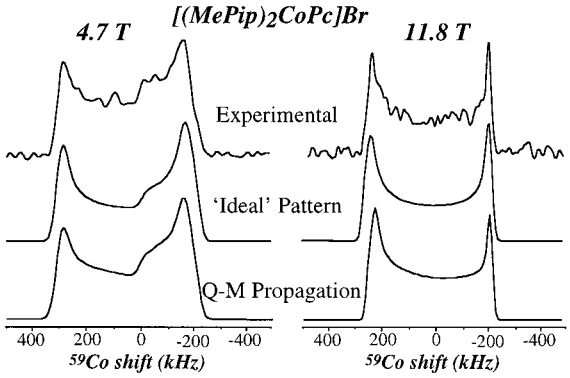

Figure 6. Field dependence observed for the solid-state ^{59}Co NMR spectrum of [(MePip)$_2$CoPc]Br. Data are as described in Figure 4 except for the fact that 200 000 scans were employed in this case for the acquisition of each subspectrum.

and second-order quadrupole anisotropies, and dipolar couplings to neighboring spins were accounted simply by a convoluting broadening. No spectroscopic evidence was found regarding the presence of chemically inequivalent sites in the complexes, and somewhat surprisingly for the case of phthalocyanines,[44] neither were polymorphs observed. Analysis of the static ^{59}Co powder patterns was then made in terms of a single ^{59}Co site; comparisons between the various experimental spectra and ideal best-fit line shape simulations calculated for the individual cobalt complexes are shown in Figures 4−7. For the sake of completeness these figures also present the simulations that for the resulting coupling parameters could be obtained from a full time propagation of the density matrix under the action of the pulse

TABLE 1: Solid-State ^{59}Co NMR Coupling Parameters Obtained for Various Co(III)phthalocyanine (Pc) and Co(III)tetraphenylporphyrin (TPP) Complexes by Iterative Line Shape Fitting

compound	e^2qQ/h (MHz)	η_Q	δ_{CSA} (ppm)	η_{CSA}	δ_{iso}[a] (ppm)	(α,β,γ)[b] (deg)
$[(Py)_2CoPc]Br$	45.0 ± 0.3	0.0 ± 0.2	-2250 ± 50	0.0 ± 0.2	7670 ± 50	(0,0,0)
$[(MeIm)_2CoPc]Br$	22.8 ± 0.3	0.3 ± 0.2	-2015 ± 50	0.2 ± 0.2	7260 ± 50	(0,0,0)
$[(MePip)_2CoPc]Br$	38.3 ± 0.3	0.1 ± 0.2	-2300 ± 50	0.1 ± 0.1	7640 ± 50	(0,0,0)
$[(NH_3)_2CoPc]Br$	8.8 ± 0.1	0.3 ± 0.1	-1160 ± 50	0.2 ± 0.1	6770 ± 50	(100,20,5)
$[(Py)_2CoTPP]BF_4$[c]	16.5 ± 0.5	0.1 ± 0.1	-1850 ± 50	0.1 ± 0.1	8430 ± 50	(0,0,0)
$[(MeIm)_2CoTPP]BF_4$[c]	3.1 ± 1.5	*d*	-1755 ± 75	0.2 ± 0.2	8632 ± 6	*d*

[a] Isotropic chemical shifts externally referenced to $\delta_{K3[Co(CN)6]} = 0$ ppm. [b] Euler angles relating quadrupolar and shielding tensors; their average error is estimated at $\pm 20°$ from repetitive line shape fittings. [c] From ref 16. [d] Quadrupolar coupling too small for accurate characterization.

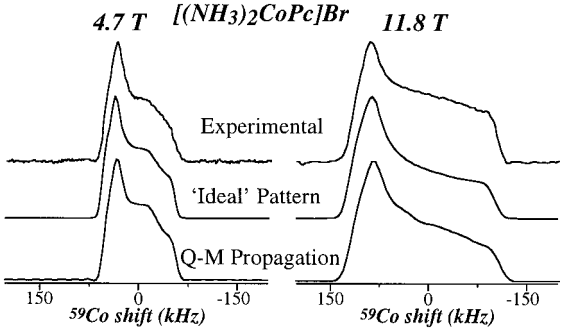

Figure 7. Field dependence observed for the solid-state ^{59}Co NMR spectrum of $[(NH_3)_2CoPc]Br$. Data are as described in Figure 4.

sequence; at most marginal differences are observed among the corresponding sets of spectra. A full listing of the quadrupolar and shielding parameters arising from these line shape fittings is presented in Table 1, together with similar parameters as recently measured for two structurally analogous porphyrin complexes. It is interesting to note that some of these cobaltophthalocyanines exhibit the largest ^{59}Co shielding and quadrupolar anisotropies reported so far for octahedral cobalt sites hexasubstituted by nitrogen bases.

When compared to the cobaltoporphyrins[16] the phthalocyanine derivatives are marked by substantial upfield isotropic shifts ($\sim$1000 ppm) that reflect subtle but systematic differences in coordination for both types of complexes. Indeed it is possible to relate these changes in ^{59}Co NMR shifts to variations in the cobalt binding via the paramagnetic 3d orbital contributions that are known to affect the metal shieldings. These contributions have an $\langle r_{3d}^{-3} \rangle$ dependence with respect to the average distance between the 3d electrons in the crystal ligand field and the metal nucleus, and the larger this nephelauxetic factor becomes the more pronounced the shielding experienced by the ^{59}Co is expected to be.[30] Although diffraction comparisons between octahedral cobaltoporphyrin and cobaltophthalocyanine complexes do not abound, data are available for one such pair, (γ-picoline)$_2$CoOEP and (γ-picoline)$_2$CoPc, which show that in the former complex $Co-N_{equatorial}$ and $Co-N_{axial}$ bonds are 0.08 and 0.09 Å longer than in the latter.[45,46] A preservation of these structural trends throughout the Co(III) complexes that are considered here could well account for the isotropic ^{59}Co NMR shifts, and it is in fact likely that should this be corroborated metal NMR could become a method of choice for achieving hitherto elusive comparisons between the geometries involved in metalloporphyrin and metallophthalocyanine complexation.[18]

All the analyzed cobaltophthalocyanines are characterized by ^{59}Co shielding and field gradient anisotropies possessing a high degree of axial symmetry and a close orientational coincidence, features that point toward the importance that the symmetry of the in-plane macrocycle has in defining these cobalt couplings. When compared with their porphyrin analogues, both the pyridine and the methylimidazole derivatives also display a large increase in their quadrupole coupling constants (30 and 20 MHz, respectively), even though the anisotropy of their chemical shieldings increases by a more modest 10−20%. It is interesting to compare this behavior with the one that has been both predicted and observed for simpler hexacoordinated cobalt complexes, where changes in shielding and quadrupolar anisotropies follow linearly one another.[29,47−49] This simple correlation is based on the assumption that the 3d orbital distribution will define not only the shielding anisotropy of the metal via paramagnetic contributions but also its local electronic field gradients.[50,51] The unusual behavior displayed by the phthalocyanine series suggests that other factors may be here at play. One such mechanism could be the hybridization of metal-based 3d orbitals and macrocycle-based π orbitals, which would then make the spectrochemical transition energy ΔE of the latter an important factor in the extent of cobalt paramagnetic deshielding. Similar 3d electron delocalization arguments but involving the aromatic orbitals of the axial ligands seem less likely, given the comparable shielding anisotropies displayed by the pyridine or methylimidazole complexes vis a vis the aliphatic ligand methylpiperidine. We are currently attempting to clarify this preliminary insight using more rigorous quantum chemical calculations of the ^{59}Co coupling parameters.

Finally, another feature worth addressing concerns the changes observed in the quadrupole coupling magnitudes throughout the series of cobalt complexes. As mentioned, these changes relate to the electronic distribution surrounding the immediate proximity of the metal. In terms of a simple partial charge model, the fact that the more strongly binding phthalocyanines introduce larger field gradients than the porphyrin ligands indicates that in these octahedral complexes the in-plane negative charge density surrounding the metal is larger than the axial one. This in turn would explain why replacing pyridines with the stronger ligand methylimidazole decreases e^2qQ/h for both Co(III)Pc and Co(III)TPP. It can also account for the substantial decrease in field gradient that then occurs upon introducing NH_3 as axial ligand, which by contrast to all the remaining ligands assayed is devoid from steric repulsions with the macrocyclic ring and can thus establish an even more intimate coordination with the metal. This stronger binding could also explain the additional isotropic upfield shift exhibited by the ^{59}Co NMR of the complex. Other features stemming from the $[(NH_3)_2CoPc]Br$ spectra are higher asymmetry parameters and a slight no-coincidence in the ^{59}Co coupling tensors. Since the higher symmetry of the presumably fast-rotating NH_3 groups should suggest an opposite trend, these features might be reflecting a distortion of the $Co-NH_3$ axis away from the normal to the macrocycle which reduces the symmetry surrounding the metal and thus accounts for this behavior.

4. Conclusions

The main objectives of this report were to describe an approach capable of yielding reliable central transition powder

line shapes even in the presence of large quadrupole couplings and to discuss its application to ^{59}Co NMR analyses of hexacoordinated phthalocyanine complexes. From a spectroscopic point of view, our approach shares several commonalties with various literature methods that use frequency-swept spin−echo acquisitions yet is also related with stochastic excitation NMR methods that minimize powder pattern distortions by relying on very weak rf excitation fields.[52] As a result of this, spectra end up freed from the actual acquisition conditions even in the presence of very large quadrupole couplings; in fact we have recently succeeded in applying such protocol to obtain distortionless line shapes from spin-5/2 powder sites with e^2qQ/h values exceeding 200 MHz.[53]

When applied to ^{59}Co, it is satisfying to note the good agreement that this powder sample approach yielded when compared to alternative magnetic resonance experiments such as pure NQR and single-crystal NMR.[15,54,55] In the case of the cobaltophthalocyanines, the usefulness of the powder NMR approach is enhanced by the difficulty in obtaining by other means the ^{59}Co NMR coupling data: phthalocyanines are poor crystal formers, and the combination of low solubility and efficient relaxation because of large molecular size and quadrupole coupling prevented us from obtaining solution spectra for some of the complexes even after extensive signal averaging at 11.8 T. Among the most interesting features revealed by the spectral parameters of the cobaltophthalocyanines is the fact that, when compared to the previously reported porphyrin derivatives, these compounds showed little change in the shielding anisotropies yet significant increases in their quadrupole couplings. Although the physical origin of these behaviors is not yet elucidated, it points toward a delocalization between the metal 3d and the macrocyclic aromatic orbitals, a behavior which we are currently exploring with the aid of quantum chemical computations of the coupling parameters.

Acknowledgment. This work was supported by the National Science Foundation through Grants DMR-9806810 and CHE-9841790 (Creativity Extension Award). L.F. is a Camille Dreyfus Teacher−Scholar (1996−2001), University of Illinois Junior Scholar (1997−2000), and Alfred P. Sloan Fellow (1997−2000).

References and Notes

(1) Cohen, M. H.; Reif, F. *Solid State Phys.* **1957**, *5*, 321.
(2) Freude, D.; Haase, J. *NMR Basic Principles Progress* **1993**, *29*, 1.
(3) Slichter, C. P. *Principles of Nuclear Magnetic Resonance*, 3rd ed.; Springer-Verlag: New York, 1990.
(4) Spiess, H. W. *Dynamic NMR Spectroscopy*; Springer-Verlag: Berlin, 1978.
(5) Abragam, A. *The Principles of Nuclear Magnetism*; Oxford University Press: Oxford, 1985.
(6) Andrew, E. R.; Bradbury, A.; Eades, R. G. *Nature* **1958**, *182*, 1659.
(7) Lowe, I. J. *Phys. Rev. Lett.* **1959**, *2*, 285.
(8) Kundla, E.; Samoson, A.; Lippmaa, E. *Chem. Phys. Lett.* **1981**, *83*, 229.
(9) Llor, A.; Virlet, J. *Chem. Phys. Lett.* **1988**, *152*, 248.
(10) Wooten, E. W.; Muller, K. T.; Pines, A. *Acc. Chem. Res.* **1992**, *25*, 209.
(11) Frydman, L.; Harwood, J. S. *J. Am. Chem. Soc.* **1995**, *117*, 5367.
(12) Medek, A.; Harwood, J. S.; Frydman, L. *J. Am. Chem. Soc.* **1995**, *117*, 12779.
(13) Stejskal, E. O.; Schaefer, J.; McKay, R. A. *J. Magn. Reson* **1977**, *25*, 569.
(14) Maricq, M. M.; Waugh, J. S. *J. Chem. Phys.* **1979**, *70*, 3300.
(15) Medek, A.; Frydman, V.; Frydman, L. *Proc. Natl. Acad. Sci. U.S.A.* **1997**, *94*, 14237.
(16) Medek, A.; Frydman, V.; Frydman, L. *J. Phys. Chem. B* **1997**, *101*, 8959.
(17) Mann, B. E.; Pregosin, P. S. In *Transition Metal NMR*; Pregosin, P. S., Ed.; Elsevier: Amsterdam, 1991; pp 143−213.
(18) Berezin, B. D. *Coordination Compounds of Porphyrins and Phthalocyanines*; J. Wiley and Sons: Salisbury, 1981.
(19) Moser, F. H.; Thomas, A. L. *The Phthalocyanines: Properties, Manufacture and Applications*; CRC Press: Boca Raton, FL, 1983.
(20) *Phthalocyanines: Properties and Applications*; Leznoff, C. C., Lever, A. B. P., Eds.; VCH Publishers: New York, 1996.
(21) See, for instance, Chapter 3 in ref 19, Vol. 2.
(22) Law, K.-Y. *Chem. Rev.* **1993**, *93*, 449.
(23) Nalwa, H. S.; Shirk, J. S. *Nonlinear Optical Properties of Metallophthalocyanines*; VCH Publishers: New York, 1996; Chapter 3, Vol. 4.
(24) Berlin, A. A.; Sherle, A. I. *Inorg. Macromol. Rev.* **1971**, *1*, 235.
(25) Serrano, J. L.; Oriol, L. *Adv. Mater.* **1995**, *7*, 348.
(26) Toscano, P. J.; Marks, T. *J. Am. Chem. Soc.* **1986**, *108*, 437.
(27) Kentgens, A. P. M.; Markis, B. A.; Vanderpol, J. F.; Nolte, R. J. M. *J. Am. Chem. Soc.* **1990**, *112*, 8800.
(28) Freeman, R.; Murray, G. R.; Richards, R. E. *Proc. R. Soc.* **1957**, *A242*, 455.
(29) Mason, J. *Chem. Rev.* **1987**, *87*, 1299.
(30) Jameson, C. J.; Mason, J. In *Multinuclear NMR*; Jameson, C. J., Mason, J., Eds.; Plenum: New York, 1987; Chapter 3.
(31) Vollmann, H.; Mertens, P. U.S. Patent 3,636,040, 1972.
(32) Mertens, P.; Vollmann, H. U.S. Patent 3,651,082, 1973.
(33) Haeberlen, U. *High-Resolution NMR in Solids*; Academic Press: New York, 1976.
(34) Chu, P. J.; Gerstein, B. *J. Chem. Phys.* **1989**, *94*, 2081.
(35) Oldfield, E.; Timken, H. K. C.; Montez, B.; Ramachandran, R. *Nature* **1985**, *318*, 163.
(36) Man, P. P. *Mol. Phys.* **1990**, *69*, 337.
(37) Haase, J.; Oldfield, E. *J. Magn. Reson. A* **1993**, *104*, 1.
(38) Massiot, D.; Farnan, I.; Gautier, N.; Trumeau, D.; Trokiner, A.; Coutures, J. P. *Solid State NMR* **1995**, *4*, 241.
(39) Dumazy, Y.; Amoureux, J.-P.; Fernandez, C. *Mol. Phys.* **1997**, *90*, 959.
(40) Agaev, Z.; Man, P. P.; Fraissard, J.; Sanctuary, B. C. *Mol. Phys.* **1997**, *91*, 75.
(41) Fenzke, D.; Freude, D.; Frohlich, T.; Haase, J. *Chem. Phys. Lett.* **1984**, *111*, 171.
(42) Man, P. P. *J. Magn. Reson.* **1986**, *67*, 78.
(43) Eichele, K.; Chan, J. C. C.; Wasylishen, R. E.; Britten, J. F. *J. Phys. Chem. A* **1997**, *101*, 5423.
(44) See, for instance, U.S. Patents 3,051,721, 3,150,150, 3,160,635, 3,357,989, and 3,708,292.
(45) Little, R. G.; Ibers, J. A. *J. Am. Chem. Soc.* **1974**, *96*, 4440.
(46) Cariati, F.; Morazzoni, F.; Zocchi, M. *Inorg. Chim. Acta* **1975**, *14*, 131.
(47) Spiess, H. W.; Haas, H.; Hartmann, H. *J. Chem. Phys.* **1969**, *50*, 3057.
(48) Chung, S. C.; Chan, J. C. C.; Au-Yeung, S. C. F.; Xu, X. *J. Phys. Chem.* **1993**, *97*, 12685.
(49) Chan, J. C. C.; Au-Yeung, S. C. F. *J. Chem. Soc., Faraday Trans.* **1996**, *92*, 1121.
(50) Lucken, E. A. C. *Nuclear Quadrupole Coupling Constants*; Academic Press: London, 1963.
(51) Brown, T. L. *Acc. Chem. Res.* **1974**, *7*, 408.
(52) Yang, D.-K.; Atkins, J. E.; Lester, C. C.; Zax, D. B. *Mol. Phys.* **1998**, *95*, 747.
(53) Wi, S.; Medek, A.; Barnes, C.; Frydman, L. Manuscript in preparation.
(54) LaRossa, R. A.; Brown, T. L. *J. Am. Chem. Soc.* **1974**, *96*, 2072.
(55) Power, W. P.; Kirby, C. W.; Taylor, N. J. *J. Am. Chem. Soc.* **1998**, *120*, 9428.